ACS OMEGA

http://pubs.acs.org/journal/acsodf

Article

Understanding the Corrosion Behavior of the AZ91D Alloy in Simulated Body Fluid through the Use of Dynamic EIS

Husnu Gerengi,* Marina Cabrini, Moses M. Solomon, and Ertugrul Kaya

Cite This: *ACS Omega* 2022, 7, 11929−11938

Read Online

ACCESS | Metrics & More | Article Recommendations

ABSTRACT: Dynamic electrochemical impedance spectroscopy (dynamic EIS) has the capacity to track changes on surfaces in a changing corrosive system, an advantage it holds over classical EIS. We used the dynamic EIS approach to provide insight into the corrosion behavior of the AZ91D Mg alloy in simulated body fluid for 30 h at 25 °C. The results reveal that the impedance response of the alloy is influenced by the immersion time. Between 0 and 7 h, impedance with three time constants was obtained, whereas two-time-constant impedance spectra were obtained between 8 and 30 h of immersion. The results confirm the breakdown of the corrosion product at longer immersion times.

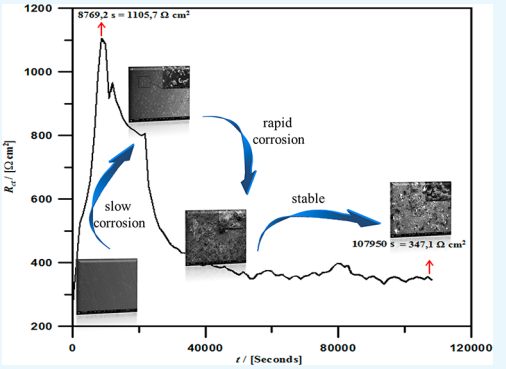

1. INTRODUCTION

Magnesium and its alloys are highly desirable in biomedical applications. They exhibit excellent biodegradable and compatible features. They also possess an elastic modulus, compressive strength, and density that are comparable to those of human bones.[1,2] Nowadays magnesium alloys are proposed as resorbable osteosynthesis devices. The possibilities to use magnesium as biodegradable orthopedic devices have been studied since the beginning of the 1900s because of the expected economic contribution to be made in this field.[3] The most interesting aspect of magnesium is its possibility to dissolve in the human body, avoiding the necessity to remove the implant after the fracture consolidation. Unfortunately, magnesium is highly reactive in human body fluids, with corrosion rates of >30−40 mm/year.[4,5] Actually there are not enough commercially available magnesium devices, but research is highly concentrated on their development.[6]

Improving the corrosion resistance property of this metal requires an in-depth understanding of the mechanism of corrosion.[7−9] Corrosion scientists have applied several corrosion-monitoring techniques to study the degradation pattern of Mg and its alloys in physiological systems. Wen et al.[5] investigated the corrosion behavior of Mg and its alloys in a modified simulated body fluid using electrochemical and surface morphological techniques. They observed that the metals heterogeneously corroded in the studied medium. Jamesh et al.[2] reported that the corrosion rate of Mg−Y−Re and Mg−Zn−Zr was higher in the initial stage of exposure to simulated body fluid and that $Ca_{10}(PO_4)_2$, $Ca_3(PO_4)_2{\cdot}3H_2O$, and $Mg(OH)_2$ were the corrosion products. Frkry and El-Sherif,[1] Liu et al.,[10] Ascencio et al.,[11] and Chen et al.[12] had also investigated the corrosion mechanism of Mg and its alloys in simulated body fluid.

Of all of the electrochemical corrosion measurement techniques used by the corrosion scientists in studying the corrosion pattern of Mg and its alloys in simulated body fluid, electrochemical impedance spectroscopy (EIS) enjoyed the highest patronage.[1,3,11,12] EIS performs reliably when three cardinal requirements of linearity, causality, and stationarity are followed.[13] The first two conditions are easily achieved, but the last is practically impossible. As such, the EIS has witnessed constant modification. The latest version of the EIS is the dynamic EIS operated in galvanostatic mode. The dynamic EIS uses short-time Fourier transform coupled with a multisinusoid perturbation signal that allows the tracking of short-term changes on a metal surface in a nonstationary system with time, temperature, and current. This technique is for now the most reliable technique for corrosion measurements since the corrosion process is dynamic in nature.[14] Detailed information pertaining to the development and workability of the dynamic EIS can be found in Darowicki et al.[15,16] as well as in Gerengi[17] and Slepski.[16,18]

Received: January 4, 2022
Accepted: March 11, 2022
Published: March 29, 2022

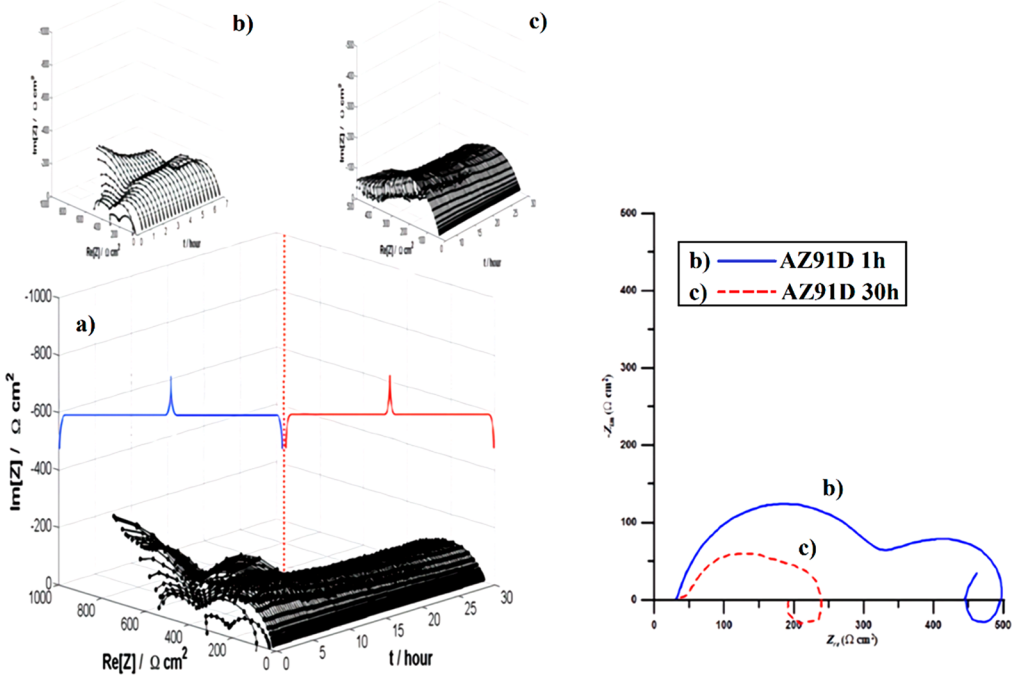

Figure 1. Plots showing changes in the electrochemical impedance spectra for the AZ91D Mg alloy in simulated body fluid with immersion time. (a) DEIS spectra after 30 h, (b) DEIS and Nyquist spectra after 0−7 h, and (c) DEIS and Nyquist spectra after 7−30 h.

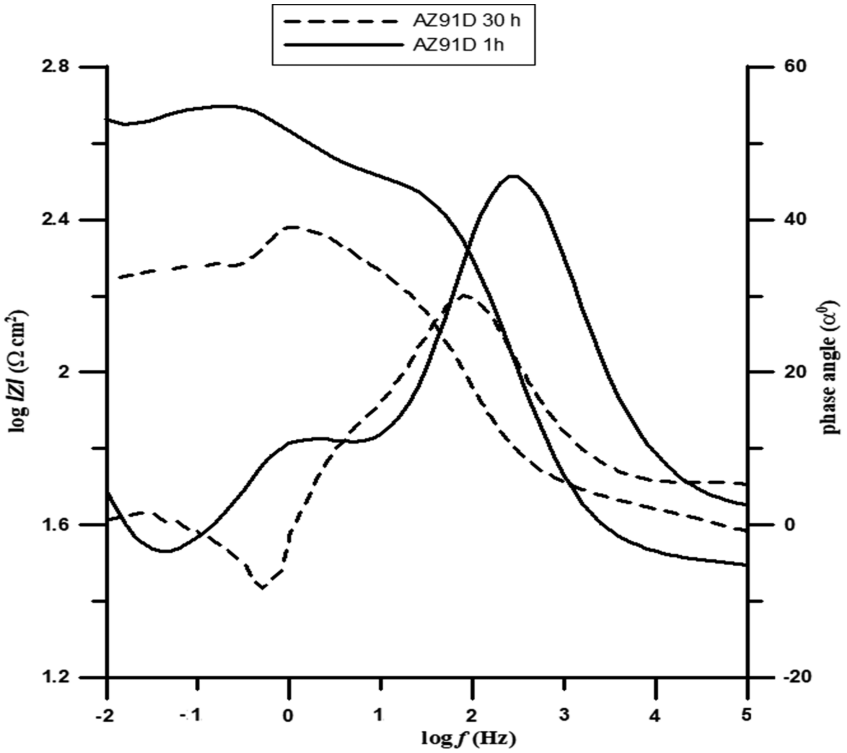

Figure 2. Bode and phase-angle plots for the AZ91D Mg alloy in simulated body fluid after 1 and 30 h of immersion time.

In this study, we apply dynamic EIS in conjunction with other techniques (potentiodynamic polarization, scanning electron microscope, and energy-dispersive spectroscopy) for the first time to study the long-term corrosion behavior of AZ91D Mg alloy in simulated body fluid. A corrosion measurement was performed for 30 h. The AZ91D Mg alloy was chosen at the expense of others because it satisfies the general requirements for biomaterials including good mechanical strength, biodegradation, and biocompatibility, and the tough dissolution of the alloy involves problems of cytocompatibility.[19]

2. RESULTS AND DISCUSSION

2.1. Dynamic EIS Studies. There is inconsistency in the impedance spectra obtained for the corrosion of Mg and its alloys in simulated body fluid, and as an effect, different

https://doi.org/10.1021/acsomega.2c00066
ACS Omega 2022, 7, 11929−11938

interpretations have been given. For the AZ91D Mg alloy in simulated body fluid, spectra with one, two, and three time constants have been reported.[1,5] The reason might not be far from the differences in the time of impedance measurements, and, most likely, the inability to achieve a stable state condition before measurements. Gawel et al.[20] recently raised an alarm about the inconsistencies in impedance diagrams and interpretations for the plasma electrolytic oxidation coating corrosion process and suggested the use of a dynamic EIS technique operated in galvanostatic mode based on continuous multisinusoidal excitation. Figure 1 presents the electrochemical impedance spectra recorded for the AZ91D Mg alloy in simulated body fluid for 30 h using the dynamic EIS approach.

As could be clearly seen in Figure 1, two kinds of spectra are present. Between 0 and 7 h (Figure 1b), spectra with two capacitive loops at high and medium frequencies and an inductive loop at low frequencies corresponding to three time constants in the Bode impedance graph (Figure 2) are seen. The capacitive loop in the high-frequency region is associated with the charge-transfer resistance (R_{ct}) and double-electric-layer capacitance at the interface.[11] The second capacitive loop in the middle frequency area corresponds to the resistance and capacitance of the electrolyte through the corrosion products on the surface of the metal. The inductive impedance loop in the low-frequency region is linked to the adsorption and breakdown of the corrosion products on the interface.[21] From 8 to 30 h (Figure 1c), a capacitive and inductive loop at high and low frequencies can be clearly identified in the spectra. The impedance arms seem to increase at low frequencies. Zhang et al.[21] had reported the possibility of the diffusive behavior of the AZ91D Mg alloy in modified simulated body fluid at longer immersion times. The presence of a diffusive effect could be explained by means of the formation of a semiprotective scale of corrosion products with a higher concentration of zinc with respect to the base alloy.[21,22] It is possible to see this effect in the Bode diagram because the modulus does not reach an asymptotic value but continually increases in the presence of an inductive loop and decreases after a maximum. Esmail et al.[23] pointed out that the parameter of interest with respect to the determination of the "real" corrosion rate is the low-frequency impedance limit, and Bland et al.[24] demonstrated it by means of EIS tests in conjunction with spectroelectrochemistry.

Figure 2 presents the Bode and phase-angle diagrams for the considered alloy after 1 h of immersion and after immersion in the test solution for 30 h. As could be seen, the value of the impedance modulus at low frequencies decreases with immersion time, indicating an increasing corrosion rate. The two-phase constants become more evident and separate, and the inductive loop shifts to lower frequencies. Following these differences in the corrosion behavior of the AZ91D Mg alloy in the investigated system with immersion time, an $R(Q(R(QR)))$ equivalent circuit was used for the analysis of the DEIS spectra obtained between 0 and 7 h, and an $R(Q(R(QR(LR))))$ equivalent circuit was used for those at 8−30 h. The equivalent circuits which are presented in Figure 3 had been previously used by Zhang et al.[21] for the analysis of EIS spectra obtained for CaP/chitosan coated on the AZ91D magnesium alloy in simulated body fluid. The R_{ct}, corrosion potential (E), and heterogeneity factor (n) obtained from this exercise were plotted as a function of immersion time to gain further insight into the corrosion process.

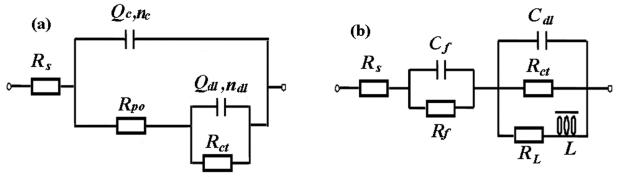

Figure 3. (a) The $R(Q(R(QR)))$ equivalent circuit was used for the analysis of the DEIS spectra obtained between 0−7 and (b) the $R(Q(R(QR(LR))))$ equivalent circuit was used for those at 8−30 h.

Figure 4a shows the variation of charge-transfer resistance of the alloy with time in the investigated system. In the referred figure, the R_{ct} sharply increased up to 1105.7 Ω cm^2 before decreasing. This is reflective of the initial rapid corrosive attack and the fast deposition of corrosion products on the alloy surface. Interestingly, at this point, the corrosion potential of the system increased steadily (Figure 4b), implying a highly perturbed system,[20,25] while the value of the n parameter decreased (Figure 4c). The R_{ct}−t (Figure 4a), n−t (Figure 4b), and E−t (Figure 4c) graphs seem to provide answers to the decrease in the diameter of the capacitive loop in the high-frequency region of Figure 1 at a longer immersion time. The decomposition of the deposited corrosion products from the alloy surface was a gradual process (Figure 4a), and this led to an increase in the heterogeneity of the surface (Figure 4b). At this time, the system potential attained quasi-stability (Figure 4c). It is pertinent to point out the fluctuating nature of the graphs in Figure 4. This is indicative of the nonstationary nature of the studied system[26,27] and thus explains the differences in the results obtained using DEIS in this study and the ones in previous studies[1,5] obtained with classical EIS.

To further demonstrate the superiority of DEIS over classical EIS, a comparison of the parameters R_p, Y_0, and n obtained under a similar experimental condition was made (Table 2). R_p is the sum of all of the resistances except the solution resistance. In Table 2, the R_p values obtained by Fekry and El-Sherif[1] and Sasikumar et al.[28] for the AZ91D Mg alloy in simulated body fluid after 1 h of immersion using the classical EIS technique are 0.50 and 0.32 kΩ cm^2 and could be said to be comparable. The Y_0 and n values rather suggest that the corrosion products deposited on AZ91D as reported by Fekry and El-Sherif[1] were more compact and homogeneous than the products on the surface reported by Sasikumar et al.[28] It should be mentioned that the Y_0 value reveals the characteristics of a surface film while the n value could be used as a measure of surface inhomogeneity.[29] These differences may not be far from the dynamic nature of the corroding system. It is obvious that DEIS is a more adaptable technique for corrosion measurements than the classical EIS technique. As can be seen in Table 1, a higher value of R_p was obtained relative to the R_p values from the EIS technique because of the better characteristics of the surface deposits as revealed by the Y_0 and n values.

2.2. PDP Studies. Figure 5 shows the PDP curves obtained for the AZ91D Mg alloy in simulated body fluid at 1 and 30 h. It is observed that the corrosion potential which is −1622.33 mV vs Ag/AgCl at 1 h of immersion increased to −1484.18 mV vs Ag/AgCl at 30 h of immersion (Table 3). The increase could be ascribed to the enrichment of the Mg−Al eutectic and the β phase, which are nobler than those for Mg, but as reported by Mathieu et al.,[30] the presence of these phases does not increase the corrosion rate because the galvanic effect is

https://doi.org/10.1021/acsomega.2c00066
ACS Omega 2022, 7, 11929−11938

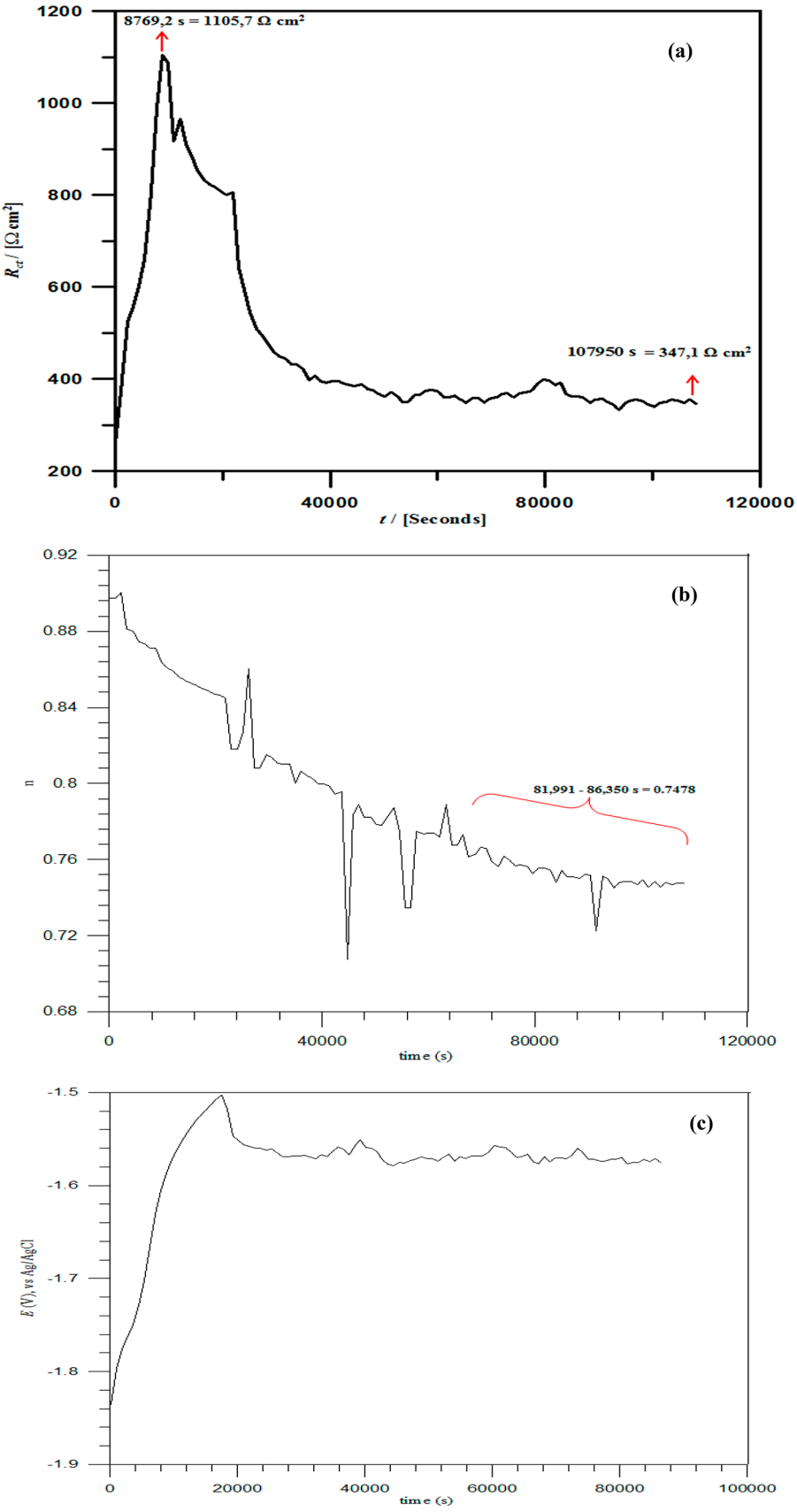

Figure 4. Plot showing the variation of (a) charge-transfer resistance, (b) the *n* parameter, and (c) the corrosion potential for the AZ91 Mg alloy in simulated body fluid with immersion time.

https://doi.org/10.1021/acsomega.2c00066
ACS Omega 2022, 7, 11929−11938

Table 1. Comparison of the Electrochemical Parameters Obtained from Classical EIS and Dynamic EIS for the AZ91D Mg Alloy in Simulated Body Fluid after 1 h of Immersion

R_p (kΩ cm^2)	Y_0 (μF cm^{-2} s n^{-1})	n	technique	reference
0.50	112.0	0.85	classical EIS	1
0.32	422.6	0.63	classical EIS	28
1.11	110.9	0.91	dynamic EIS	present work

very small. On the contrary, other authors[31−34] take the view that the typical microstructure of this alloy has a primary α phase and a divorced eutectic which consists of the β phase ($Mg_{17}Al_{12}$) and that the eutectic β phase distributed along α-phase grain boundaries produced Al enrichment on the corroded surface, which may be the key factors that limit the progression of corrosion damage. Wang et al.[34] identified the presence of $Mg(OH)_2$, $Mg_5(CO_3)_4(OH)_2{\cdot}8H_2O$, and MgO phases in the corrosion products, but only the latter two phases were found in the passive film.

Further examination of the polarization curve at 1 h reveals that the anodic branch exhibits passivity which breaks down at a potential of −1454 mV vs Ag/AgCl. The passivity and the breakdown potential are not observed in the polarization curve at 30 h, and the corrosion current density decreased from 46.88 to 45.29 μA/cm^2 (Table 2). Consequently, the instantaneous corrosion rate ($CR_i = 22.85 \times i_{corr}$)[28] decreased from 1.06 mm/year at 1 h of immersion to 1.02 mm/year at 30 h of immersion. According to Wang et al.,[34] such declines in i_{corr} and CR_i could mean that pits on the surface were quickly passivated by the deposited surface films around the area of the pits such that current flowing through the pits at increasing polarization time was hindered.

The dissolution of Mg in an aqueous environment is complicated. Song and Atrens[35] summarized the process as follows (eqs 1−4):

$$2H_2O + 2e^- \rightarrow H_2 + 2OH^- \text{ (cathodic reaction)} \quad (1)$$

$$Mg \rightarrow Mg^{+2} + 2e^- \text{ (anodic reaction)} \quad (2)$$

$$Mg + 2H_2O \rightarrow Mg(OH)_2 + H_2 \text{ (overall reaction)} \quad (3)$$

$$Mg^{2+} + 2OH^- \rightarrow Mg(OH)_2 \text{ (product formation)} \quad (4)$$

As implied by eq 2, at the substrate/electrolyte interface, Mg is oxidized to the Mg^{2+} intermediate. The ion intermediate reacts chemically with H_2O to form OH^- and H_2 (eqs 2 and 3). During the degradation process, the electrolyte pH increases, as could be seen in Figure 6 as a result of the accumulation of OH^- ions, and the effect is the formation of corrosion products, $Mg(OH)_2$ (eq 4). As mentioned earlier, $Mg(OH)_2$ exhibits a partial corrosion suppression effect which is lost in a corrosive system containing halide ions according to eq 5.[11]

$$Mg(OH)_2 + 2Cl^- \rightarrow Mg^{2+} + 2Cl^- + 2OH^- \quad (5)$$

2.3. Hydrogen Evolution Studies. Figure 7 shows the variation of hydrogen gas evolution with time during the degradation of AZ91D Mg alloy corrosion in SBF at 25 and 37 °C. A linear relationship is observed, implying that the volume of hydrogen gas that is evolved increases with increasing time. As should be expected, the metal degraded more rapidly at 37 °C than at 25 °C, leading to a higher volume of gas evolution. The calculated dissolution rate (v_d, cm^3 h^{-1}) (eq 6) values are 1.37 and 1.68 cm^{-2} h^{-1} at 25 and 37 °C, respectively. These results are in agreement with the value report by Vrsalović et al.[36] The authors had demonstrated that increasing temperature increases the corrosion rate of Mg in body fluid.

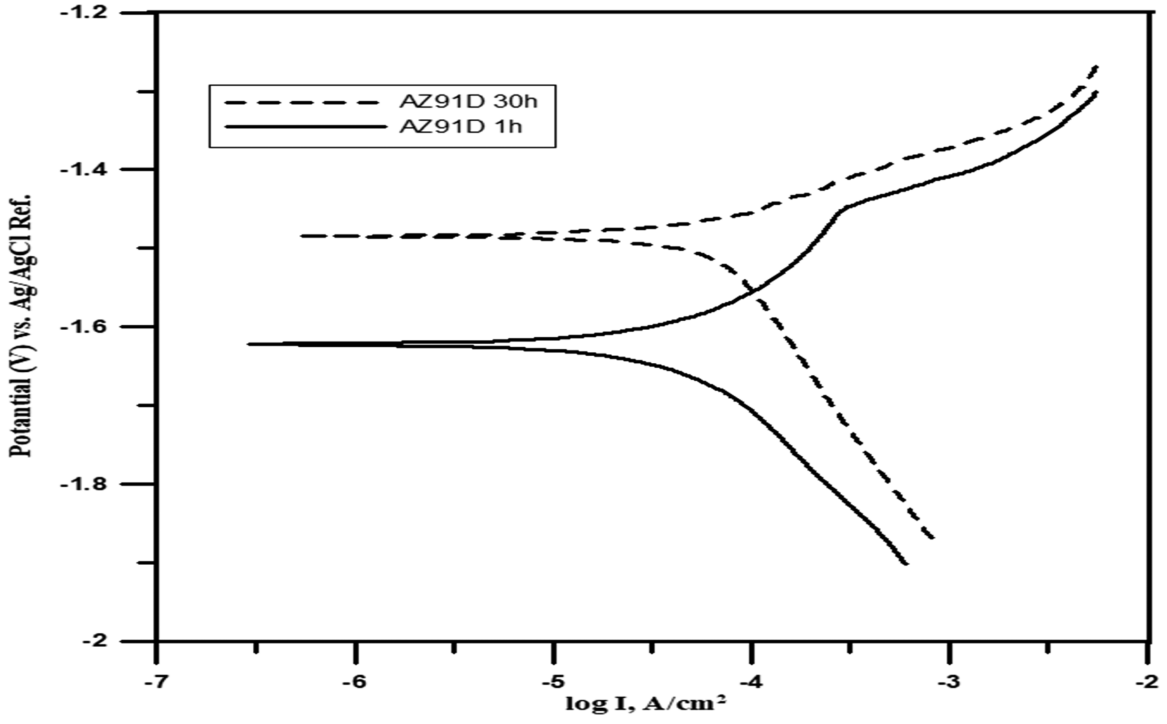

Figure 5. Potentiodynamic polarization curves obtained for the AZ91 Mg alloy in simulated body fluid at 1 h and 30 h.

https://doi.org/10.1021/acsomega.2c00066
ACS Omega 2022, 7, 11929−11938

Table 2. Potentiodynamic Polarization Parameters for the AZ91D Mg Alloy in Simulated Body Fluid

immersion time (h)	$-E_{corr}$ (mV/Ag/AgCl)	i_{corr} (μA cm^{-2})	β_c (mV dec^{-1})	β_a (mV dec^{-1})	CR_i (mm/year)
1	1622.3	46.88	249.4	199.0	1.06
30	1484.2	45.29	205.7	87.1	1.02

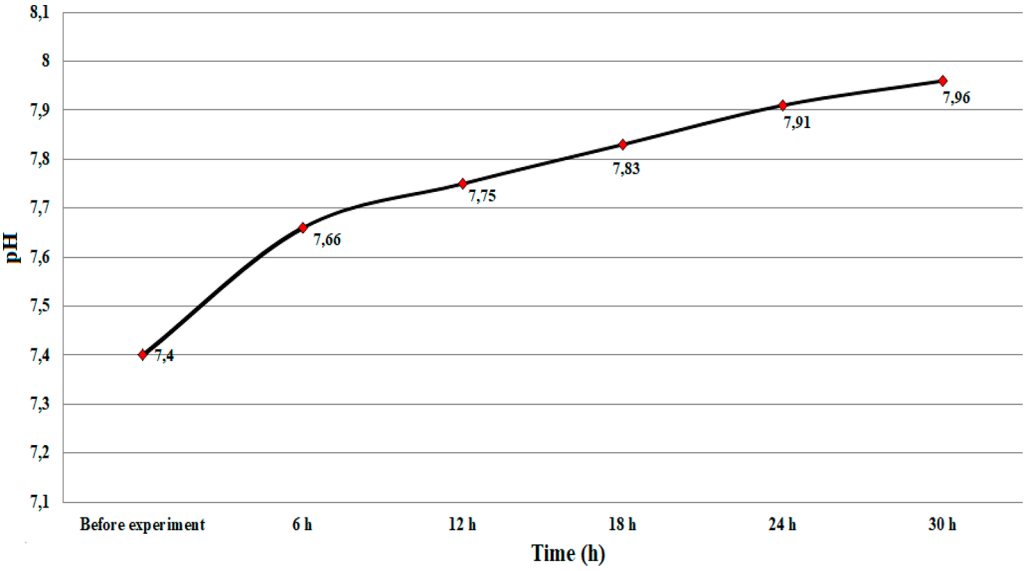

Figure 6. pH values of simulated body fluid containing the AZ91 Mg alloy at different exposure times

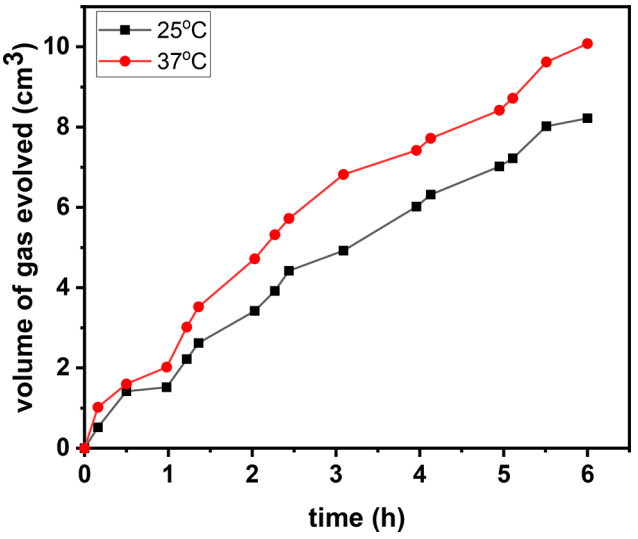

Figure 7. Variation of the volume of H_2 evolved with time during AZ91D Mg alloy corrosion in SBF at 25 and 37 °C.

2.4. SEM and EDAX Studies. Pictures of AZ91D Mg alloy taken in (a) the abraded state and after immersion in simulated body fluid for (b) 6, (c) 12, (d) 18, (e) 24, and (f) 30 h at ambient temperature are displayed in Figure 8. The corresponding EDAX results are given in Figure 9. The smoothness of the surface in the abraded state (Figure 8a) is lost to corrosion after immersion in simulated body fluid (Figure 8b–f). The surface in Figure 8b is characterized by cracks, and the higher-magnification image inserted into the figure reveals a layer of deposited products on the surface. The dissolution and breakdown of the deposited layer become obvious with increasing immersion time (Figure 8b–f). Pits of varying depth can be seen in Figure 8b–f. These SEM results contradict the results by Fekry and El-Sherif.[1] The authors had concluded from their SEM images that the formation of a complete surface layer of oxidation products on the AZ91D Mg alloy was difficult after 35 h of immersion in simulated body fluid.

The EDAX spectra and the inserted elemental composition table in Figure 9a suggest absence of oxides on the alloy surface after abrasion. Elements Ca, Cl, O, P, K, and C are found in Figure 9b–f but not in Figure 9a, meaning that these elements were adsorbed onto the surface after interaction with simulated body fluid. Several research works have established that insoluble phosphates, carbonates, MgO, and $Mg(OH)_2$ are the major components of the corrosion product on Mg and its alloy when exposed to simulated body fluid.[28,11,37] It is observed from the insert tables in Figure 9b–f that O is present in the highest percentage among all of the adsorbed elements. This may mean a larger amount of oxides in the corrosion products compared to the quantities of carbonates and phosphates. According to Liu et al.'s[10] findings, Mg alloy corrosion in simulated body fluid produced, in addition to $MgO/Mg(OH)_2$, phosphate/carbonate compounds and confers a different protective characteristics to the film relative to the characteristics of the film formed on a Mg surface in pure chloride-containing solution. Hence, the change in phosphate/carbonate compounds, with respect to composition, thickness, and morphology as time elapses, is capable of contributing substantially to the protection of magnesium alloys against further dissolution.

3. SUMMARY

The AZ91D Mg alloy is versatile because of its excellent combination of mechanical, corrosion, and castability properties, hence gaining wide application as orthopedic devices[38−40] and as inflammatory host responses.[41] A large amount of research has been devoted to understanding the corrosion

https://doi.org/10.1021/acsomega.2c00066
ACS Omega 2022, 7, 11929−11938

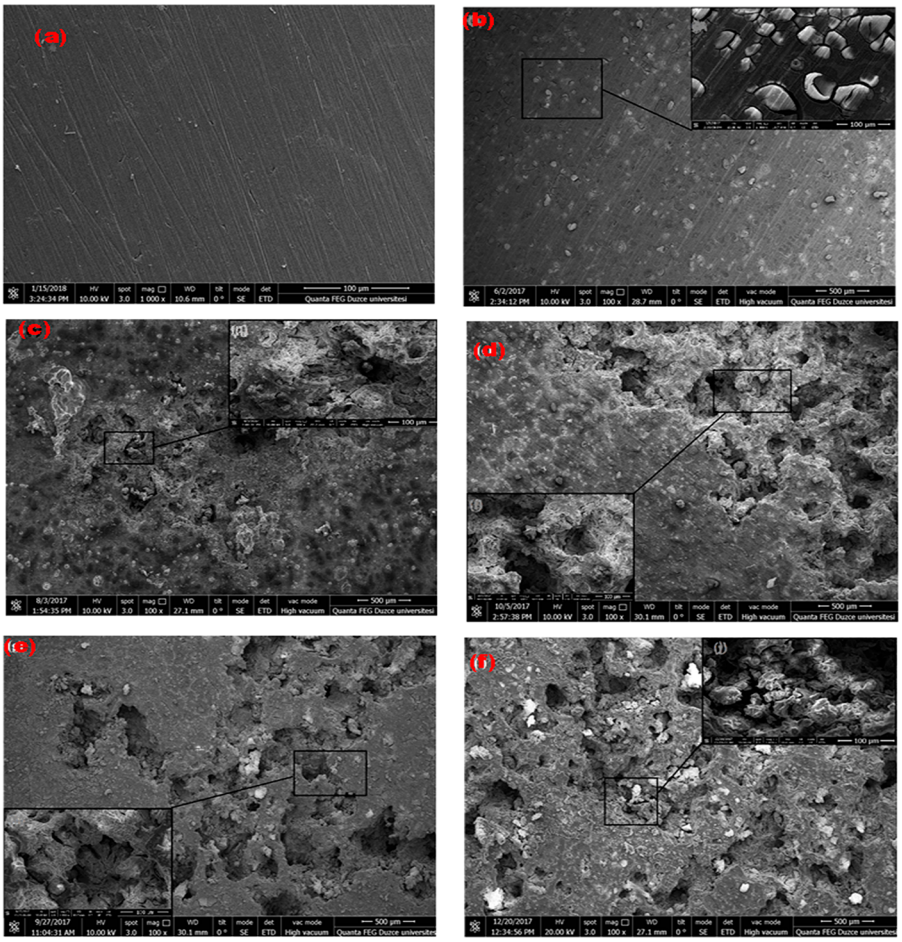

Figure 8. SEM images for the AZ91D magnesium alloy in (a) the abraded state and after immersion in simulated body fluid for (b) 6, (c) 12, (d) 18, (e) 24, and (f) 30 h at 25 °C.

behavior of this alloy, most of which used the classical EIS technique.[1,5,19,28] Inconsistent results and divergent opinions and interpretations are given.[1,5] We have used the dynamic EIS approach to gain more insight into the corrosion behavior of the the AZ91D Mg alloy in simulated body fluid. Our dynamic EIS results reveal that the impedance response of the AZ91D alloy is influenced by the immersion time. Impedance spectra with three time constants are obtained at between 0 and 7 h, and impedance spectra with two time constants are obtained at between 8 and 30 h of immersion in simulated body fluid. SEM and EDAX results give a clear picture of severe damage to the alloy in the studied medium. In the early stage of corrosion, products generated from the process exhibit an inhibiting effect according to the $R_{ct}-t$ diagram. The $E-t$ plot discloses that the corrosion system is not a stable system, particularly at the early stage, but assumes false stability at a longer immersion time. This explains the inconsistencies in the results reported from the classical EIS technique.[1,5] Hydrogen evolution results show a linear relationship between the volume of hydrogen gas evolved with time.

4. EXPERIMENTAL DETAILS

Disc-shaped specimens of the AZ91D Mg alloy were cut out of an AZ91D sheet having chemical compositions by percentage weight as follows: Al 8.77, Zn 0.74, Mn 0.18, Si <0.01, Fe <0.001, Cu <0.001, Ca <0.01, Ni 0.001, and the remainder as Mg. Thereafter, some parts of the samples were covered with epoxy resin so as to get 0.785 cm^2 as the surface area of the exposed surface. Prior to electrochemical measurements, the specimens were wet abraded mechanically with emery paper grit nos. 800, 1200, 1500, 1800, and 2000 and dried with warm air.

The simulated body fluid (SBF) solution was prepared by following the procedure reported by Kokubo et al.[42] and Sasikumar et al.[28] The chemicals and the amounts used for SBF preparation are given in Table 3. Preparation was carried out at ambient temperature (25 °C).

The dynamic EIS measurements were performed with a setup described by Slepki et al.[43] The generation of the current perturbation was accomplished through the use of a National Instruments Ltd. PCI-4461 digital−analog card. The card also performed the task of recording current and voltage signals.[44,45] The excitation signal had the form of the sum of current sinusoids over the range of 4.5 kHz−700 mHz. The corrosion processes of the Mg alloy were recorded for 30 h. At the end of each dynamic EIS experiments, samples were submitted for surface morphology examination, and this examination was performed using energy-dispersive X-ray spectroscopy (EDAX) coupled to scanning electron microscopy (SEM; J. Quanta FEG 250 model; FEI, Holland).

For potentiodynamic polarization (PDP) experiments, measurements were performed in a standard three-electrode electrochemical cell. A potentiostat/galvanostat/ZRA (Reference 600) Gamry instrument embedded with a Gamry

https://doi.org/10.1021/acsomega.2c00066
ACS Omega 2022, 7, 11929−11938

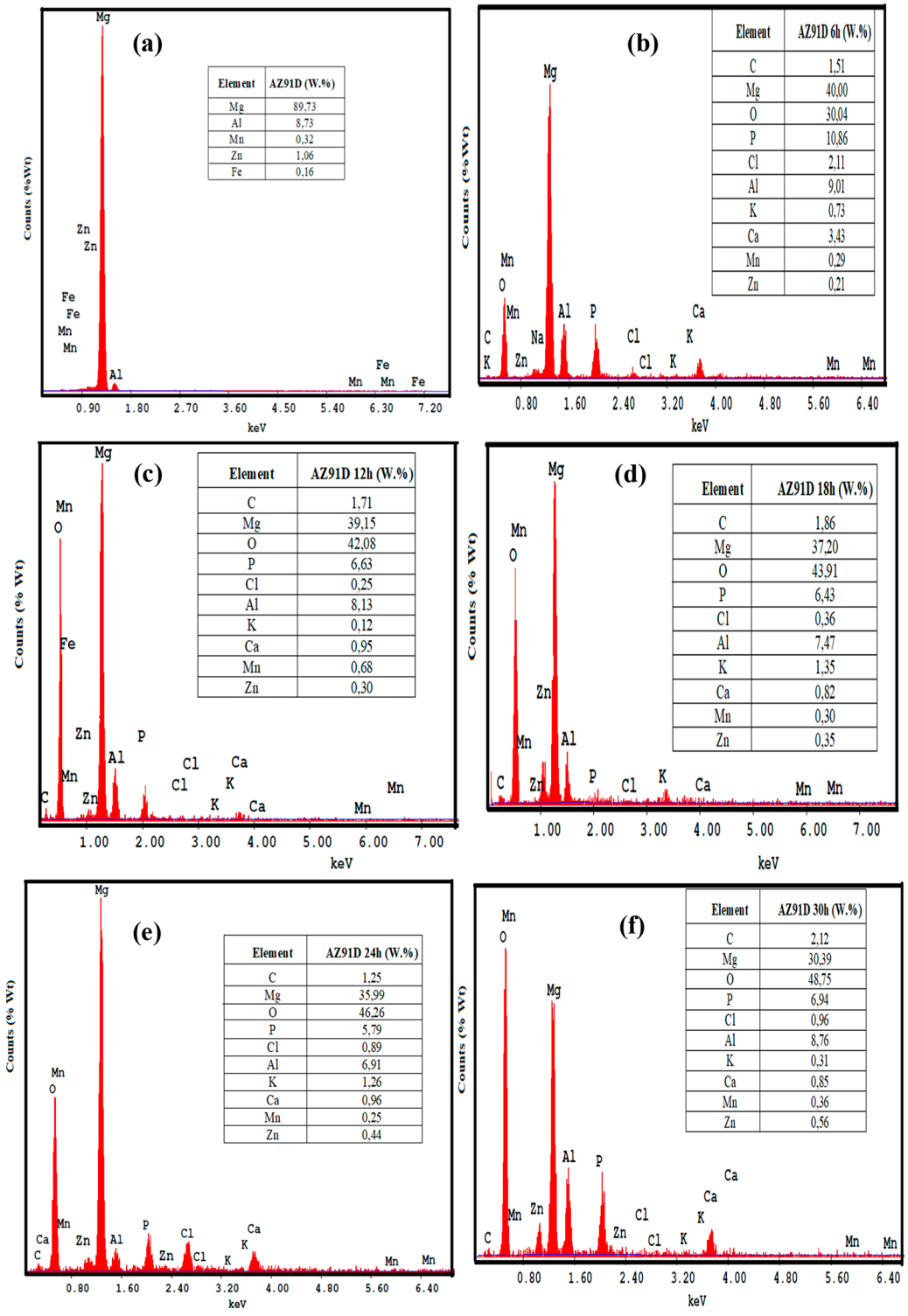

Figure 9. EDAX spectra of the AZ91D magnesium alloy in (a) the abraded state and after immersion in simulated body fluid for (b) 6, (c) 12, (d) 18, (e) 24, and (f) 30 h at 25 °C. Each inset shows the elemental composition.

framework system composed of the ESA410 software application was used. The prepared AZ91D Mg alloy served as the working electrode, Ag/AgCl was the reference electrode, and a platinum plate played the role of a counter electrode. The potential was swept from the negative direction to the positive direction at a constant sweep rate of 1 mV/s from −250 to +250 mV relative to the corrosion potential (E_{corr}). The corrosion current density (I_{corr}) and E_{corr} were obtained by Tafel fitting using EC-lab software.

It is generally accepted that eq 3 is the overall corrosion reaction of magnesium and its alloys. $H_2(g)$ in eq 3 can be used as an indicator of the rate of corrosion of the metal.[46] The rate of dissolution of the AZ91D Mg alloy immersed in SBF was studied by monitoring the volume of gas produced for 6 h. The dissolution rate (v_d, $cm^3\ h^{-1}$) was calculated using eq 6:[47]

https://doi.org/10.1021/acsomega.2c00066
ACS Omega 2022, 7, 11929−11938

Table 3. Chemical Composition of SBF

S/N	chemical	amount (g/1000 mL)
1	NaCl	8.035
2	$NaHCO_3$	0.355
3	KCl	0.225
4	$K_2HPO_4{\cdot}3H_2O$	0.231
5	$MgCl_2{\cdot}H_2O$	0.311
6	1 M HCl	40 mL
7	$CaCl_2$	0.292
8	Na_2SO_4	0.072
9	$((CH_2OH)_3CNH_2)$	6.118
10	1 M HCl	appropriate amount for adjusting to pH 7.4

$$\nu_d = \frac{V_t - V_i}{t_t - t_i} \quad (6)$$

where V_t is the volume of gas liberated at final time t_t (6 h) and V_i is the volume of gas generated at initial time t_i (0 h).

AUTHOR INFORMATION

Corresponding Author

Husnu Gerengi − *Corrosion Research Laboratory, Department of Mechanical Engineering, Faculty of Engineering, Düzce University, 81620 Düzce, Turkey; Department of Engineering and Applied Sciences, University of Bergamo, 24044 Bergamo, BG, Italy;* orcid.org/0000-0002-9663-4264; Email: husnugerengi@duzce.edu.tr

Authors

Marina Cabrini − *Department of Engineering and Applied Sciences, University of Bergamo, 24044 Bergamo, BG, Italy*

Moses M. Solomon − *Department of Chemistry, College of Science and Technology, Covenant University, 112104 Ota, Ogun State, Nigeria*

Ertugrul Kaya − *Corrosion Research Laboratory, Department of Mechanical Engineering, Faculty of Engineering, Düzce University, 81620 Düzce, Turkey;* orcid.org/0000-0003-1579-6411

Complete contact information is available at: https://pubs.acs.org/10.1021/acsomega.2c00066

Notes

The authors declare no competing financial interest.

ACKNOWLEDGMENTS

Husnu Gerengi expresses his sincere thanks to The Scientific and Technological Research Council of Turkey (TUBITAK) for his fellowship at the University of Bergamo under the TUBITAK 2219 Postdoctoral Research program (program project number 1059B191900111).

REFERENCES

(1) Fekry, A. M.; El-Sherif, R. M. Electrochemical corrosion behavior of magnesium and titanium alloys in simulated body fluid. *Electrochim. Acta* **2009**, *54*, 7280−7285.

(2) Jamesh, M. I.; Wu, G.; Zhao, Y.; McKenzie, D. R.; Bilek, M. M. M.; Chu, P. K. Electrochemical corrosion behavior of biodegradable Mg-Y-RE and Mg-Zn-Zr alloys in Ringer's solution and simulated body fluid. *Corros. Sci.* **2015**, *91*, 160−184.

(3) Witte, F. The history of biodegradable magnesium implants: A review. *Acta Biomater* **2010**, *6*, 1680−1692.

(4) Acheson, J. G.; Gallagher, E. A.; Ward, J.; McKillop, S.; Fitz Gibbon, B.; Boyd, A. R.; Meenan, B. J.; Lemoine, P.; McGarry, J. P. Shear testing and failure modelling of calcium phosphate coated AZ31 magnesium alloys for orthopaedic applications. *Surf. Coat. Technol.* **2022**, *429*, 127944.

(5) Wen, Z.; Wu, C.; Dai, C.; Yang, F. Corrosion behaviours of Mg and its alloys with different Al contents in a modified simulated body fluid. *J. Alloys Compd.* **2009**, *488*, 392−399.

(6) Sonnow, L.; Könneker, S.; Vogt, P. M.; Wacker, F.; Falck, C. Biodegradable magnesium Herbert screw − image quality and artifacts with radiography. CT and MRI. *BMC Med. Imaging* **2017**, *17*, 16.

(7) Ghafarzadeh, M.; Kharazih, M.; Atapour, M. Bilayer micro-arc oxidation-poly (glycerol sebacate) coating on AZ91 for improved corrosion resistance and biological activity. *Prog. Org. Coat.* **2021**, *161*, 106495.

(8) Dalmoro, V.; Azambuja, D. S.; Aleman, C.; Armelin, E. Hybrid organophosphonic-silane coating for corrosion protection of magnesium alloy AZ91: The influence of acid and alkali pre-treatments. *Surf. Coat. Technol.* **2019**, *357*, 728−739.

(9) Merlo, J. L.; Katunar, M. R.; de la Hoz, M. F. T.; Carrizo, S.; Alonso, L. S.; Otaz, M. A.; Ballarre, J.; Ceré, S. Short-Term in vivo response to anodized magnesium alloy as a biodegradable material for bone fracture fixation devices. *ACS Appl. Bio Mater.* **2021**, *4*, 7123−7133.

(10) Liu, Y.; Curioni, M.; Liu, Z. Correlation between electrochemical impedance measurements and corrosion rates of Mg-1Ca alloy in simulated body fluid. *Electrochim. Acta* **2018**, *264*, 101−108.

(11) Ascencio, M.; Pekguleryuz, M.; Omanovic, S. An investigation of the corrosion mechanisms of WE43 Mg alloy in a modified simulated body fluid solution: The effect of electrolyte renewal. *Corros. Sci.* **2015**, *91*, 297−310.

(12) Chen, X. B.; Li, C.; Xu, D. Biodegradation of Mg-14Li alloy in simulated body fluid: A proof-of-concept study. *Bioact. Mater.* **2018**, *3*, 110−117.

(13) Solomon, M. M.; Gerengi, H.; Umoren, S. A. Carboxymethyl cellulose/silver nanoparticles composite: Synthesis, characterization, and application as a benign corrosion inhibitor for St37 steel in 15% H_2SO_4 medium. *ACS Appl. Mater. Interfaces* **2017**, *9*, 6376−6389.

(14) Rizvi, M.; Gerengi, H.; Gupta, P. Experimental Methods of Corrosion Inhibition Assessment. *Sustainable Corrosion Inhibitors I: Fundamentals, Methodologies, and Industrial Applications*; ACS Symposium Series; American Chemical Society: Washington, D.C., 2021; Vol. *1403*, Chapter 4, pp 49−60.

(15) Darowicki, K.; Slepski, P.; Szocinski, M. Application of the dynamic EIS to investigation of transport within organic coatings. *Prog. Org. Coat.* **2005**, *52*, 306−310.

(16) Darowicki, K.; Slepski, P. Dynamic electrochemical impedance spectroscopy of the first order electrode reaction. *J. Electroanal. Chem.* **2003**, *547*, 1−8.

(17) Gerengi, H. The use of dynamic electrochemical impedance spectroscopy in corrosion inhibitor studies. *Prot. Met. Phys. Chem. Surf.* **2018**, *54*, 536−540.

(18) Darowicki, K.; Slepski, P. Instantaneous electrochemical impedance spectroscopy of electrode reactions. *Electrochim. Acta* **2004**, *49*, 763−772.

(19) Gu, X. N.; Zhou, W. R.; Zheng, Y. F.; Cheng, Y.; Wei, S. C.; Zhong, S. P.; Xi, T. F.; Chen, L. J. Corrosion fatigue behaviors of two biomedical Mg alloy − AZ91D and WE43 − In simulated body fluid. *Acta Biomater* **2010**, *6*, 4605−4613.

(20) Gawel, L.; Nieuzyl, L.; Nawrat, G.; Darowicki, K.; Slepski, P. Impedance monitoring of corrosion degradation of plasma electrolytic oxidation coatings (PEO) on magnesium alloy. *J. Alloys Compd.* **2017**, *722*, 406−413.

(21) Zhang, J.; Dai, C.; Wen, Z.; Wei, J. Study on the effect of the coating thickness on corrosion behavior of AZ91D magnesium alloy in m-SBF. *Int. J. Electrochem. Sci.* **2015**, *10*, 6002−6013.

(22) Chang, J. W.; Guo, X. W.; He, S. M.; Fu, P. H.; Peng, L. M.; Ding, W. J. Investigation of the corrosion for Mg−*x*Gd−3Y−0.4Zr (*x* = 6, 8, 10, 12 wt%) alloys in a peak-aged condition. *Corros. Sci.* **2008**, *50*, 166−177.

(23) Esmaily, M.; Svensson, J. E.; Fajardo, S.; Birbilis, N.; Frankel, G. S.; Virtanen, S.; Arrabal, R.; Thomas, S.; Johansson, L. G. Fundamentals and advances in magnesium alloy corrosion. *Prog. Mater. Sci.* **2017**, *89*, 92−193.
(24) Bland, L. G.; Scully, L. C.; Scully, J. R. Assessing the corrosion of multi-phase Mg-Al alloys with high Al content by electrochemical impedance, mass loss, hydrogen collection, and inductively coupled plasma optical emission spectrometry solution analysis. *Corrosion* **2017**, *73*, 526−543.
(25) Darowicki, K.; Slepski, P.; Szocinski, M. Application of the dynamic EIS to investigation of transport within organic coatings. *Prog. Org. Coat.* **2005**, *52*, 306−310.
(26) Gerengi, H.; Jazdzewska, A.; Kurtay, M. A comprehensive evaluation of mimosa extract as a corrosion inhibitor on AA6060 alloy in acid rain solution: part I. Electrochemical AC methods. *J. Adhes. Sci. Technol.* **2015**, *29*, 36−48.
(27) Gerengi, H.; Mielniczek, M.; Gece, G.; Solomon, M. M. Experimental and quantum chemical evaluation of 8-hydroxyquinoline as a corrosion inhibitor for copper in 0.1 M HCl. *Ind. Eng. Chem. Res.* **2016**, *55*, 9614−9624.
(28) Sasikumar, Y.; Solomon, M. M.; Olasunkanmi, L. O.; Ebenso, E. E. Effect of surface treatment on the bioactivity and electrochemical behavior of magnesium alloys in simulated body fluid. *Mater. Corros* **2017**, *68*, 776−790.
(29) Sha, J. Y.; Ge, H. H.; Wan, C.; Wang, L. T.; Xie, S. Y.; Meng, X. J.; Zhao, Y. Z. Corrosion inhibition behaviour of sodium dodecyl benzene sulphonate for brass in an Al_2O_3 nanofluid and simulated cooling water. *Corros. Sci.* **2019**, *148*, 123−33.
(30) Mathieu, S.; Rapin, C.; Steinmetz, J.; Steinmetz, P. A corrosion study of the main constituent phases of AZ91 magnesium alloys. *Corros. Sci.* **2003**, *45*, 2741−2755.
(31) Pardo, A.; Merino, M. C.; Coy, A. E.; Viejo, F.; Arrabal, R.; Feliú, S., Jr. Influence of microstructure and composition on the corrosion behaviour of Mg/Al alloys in chloride media. *Electrochim. Acta* **2008**, *53*, 7890−902.
(32) Pardo, A.; Merino, M. C.; Coy, A. E.; Arrabal, R.; Viejo, F.; Matykin, E. Corrosion behaviour of magnesium/aluminium alloys in 3.5 wt% NaCl. *Corros. Sci.* **2008**, *50*, 823−834.
(33) Song, G.; Bowles, A. L.; StJohn, D. H. Corrosion resistance of aged die cast magnesium alloy AZ91D. *Mater. Sci. Eng., A* **2004**, *366*, 74−86.
(34) Wang, L.; Zhang, B. P.; Shinohara, T. Corrosion behavior of AZ91 magnesium alloy in dilute NaCl solutions. *Mater. Des* **2010**, *31*, 857−863.
(35) Song, G.; Atren, A. Corrosion mechanism of magnesium alloys. *Adv. Eng. Mater.* **1999**, *1*, 11−33.
(36) Vrsalović, L.; Kliškić, M.; Radošević, J.; et al. *J. Appl. Electrochem.* **2005**, *35*, 1059−1065.
(37) Wang, B. J.; Xu, D. K.; Dong, J. H.; Ke, W. Effect of corrosion product films on the in vitro degradation of Mg-3%Al-1%Zn (in wt%) alloy in Hank's solution. *J. Mater. Sci. Technol.* **2018**, *34*, 1756−1764.
(38) Kannan, M. B.; Raman, R. K. S. Evaluating the stress corrosion cracking susceptibility of Mg−Al−Zn alloy in modified-simulated body fluid for orthopaedic implant application. *Scr. Mater.* **2008**, *59*, 175−178.
(39) Witte, F.; Ulrich, H.; Palm, C.; Willbold, E. Biodegradable magnesium scaffolds. Part II. Peri-implant bone remodeling. *J. Biomed. Mater. Res., Part A* **2007**, *81*, 757−765.
(40) Majumdar, J. D.; Bhattacharyya, U.; Biswas, A.; Manna, I. Studies on thermal oxidation of Mg-alloy (AZ91) for improving corrosion and wear resistance. *Surf. Coat. Technol.* **2008**, *202*, 3638−42.
(41) Witte, F.; Ulrich, H.; Rudert, M.; Willbold, E. Biodegradable magnesium scaffolds. Part I. Appropriate inflammatory response. *J. Biomed. Mater. Res., Part A* **2007**, *81*, 748−756.
(42) Kokubo, T.; Takadama, H. How useful is SBF in predicting in vivo bone bioactivity? *Biomaterials* **2006**, *27*, 2907−2915.
(43) Slepski, P.; Gerengi, H.; Gece, G.; Kaya, E.; Rizvi, M.; Szocinski, M. Electrochemical Evaluation of Sustainable Corrosion Inhibitors via Dynamic Electrochemical Impedance Spectroscopy. *Sustainable Corrosion Inhibitors I: Fundamentals, Methodologies, and Industrial Applications*; ACS Symposium Series; American Chemical Society: Washington, D.C., 2021; Vol. *1403*, Chapter 5, pp 61−85.
(44) Gerengi, H.; Darowicki, K.; Bereket, G.; Slepski, P. Evaluation of corrosion inhibition of brass-118 in artificial seawater by benzotriazole using dynamic EIS. *Corros. Sci.* **2009**, *51*, 2573−2579.
(45) Gerengi, H.; Tascioglu, C.; Akcay, C.; Kurtay, M. Impact of copper chrome boron (CCB) wood preservative on the corrosion of St37 steel. *Ind. Eng. Chem. Res.* **2014**, *53*, 19192−19198.
(46) Saji, V. S. Organic conversion coatings for magnesium and its alloys. *J. Ind. Eng. Chem.* **2019**, *75*, 20−37.
(47) Umoren, S. A.; Solomon, M. M.; Udosoro, I. I.; Udoh, A. P. Inhibitive and adsorption behaviour of carboxymethyl cellulose on mild steel corrosion in sulphuric acid solution. *Corros. Sci.* **2010**, *52*, 1317−1325.

https://doi.org/10.1021/acsomega.2c00066
ACS Omega 2022, 7, 11929−11938